International Journal of Solids and Structures 248 (2022) 111686

Contents lists available at ScienceDirect

International Journal of Solids and Structures

journal homepage: www.elsevier.com/locate/ijsolstr

Prediction of the overall mechanical response of gradient nano-grained materials based on grain size distribution profile

Li Yu

State Key Laboratory of Nonlinear Mechanics, Institute of Mechanics, Chinese Academy of Sciences, Beijing 100190, China

ARTICLE INFO

Keywords:
Constitutive modeling
Grain size distribution
Strength
Ductility
Gradient structured metals

ABSTRACT

Inspired by the gradient structure of biological materials, various gradient nano-grained (GNG) materials, inside which grain size spans several orders of magnitude, have been manufactured in recent years. This kind of material often exhibits extra hardening ability and ultimately achieves synergetic strength and ductility. The extra hardening of GNG materials is closely related to the strain gradient formed during deformation. However, the analytical relation between the structural gradient, strain gradient is still unexplored. Besides, the previous works focused on only one type of GNG material, and the understanding of the effect of different kinds of microstructures is limited. This paper explores the analytical relations between the strain gradient and the average grain size, as well as the grain size gradient in GNG materials. The overall mechanical responses of GNG interstitial-free (IF) steel and GNG Ni are well predicted. The results verify that the extra hardening of GNG materials is dependent on their unique microstructures. The strength and ductility of GNG materials can be improved by adjusting the composition and distribution of coarse grains and nano-grains.

1. Introduction

The strength-ductility trade-off dilemma has long been the bottleneck in developing metallic structured materials, especially ultra-high strength. Therefore, significant efforts have been made to find a way to enhance both strength and ductility of materials over several decades. Inspired by the gradient structures of biological materials, researchers have manufactured various GNG materials in recent years (Li et al., 2020; Wu and Fan, 2020; Wu et al., 2020). The average grain size of these GNG materials changes from the sample surface into its interior by four orders of magnitude. This class of material exhibits superior mechanical properties, including strength-ductility synergy, extraordinary strain hardening, and fatigue resistance (Cheng et al., 2018; Fang et al., 2011; Lin et al., 2018; Long et al., 2019; Lu, 2014; Shao et al., 2017; Wei et al., 2014; Wu et al., 2014). For example, GNG Cu prepared through surface mechanical grinding treatment (SMAT) exhibits a doubling yield strength to that of the coarse-grained (CG), meanwhile preserving a ductility of about 30% (Fang et al., 2011). Similar results can also be found in the GNG IF steel (Wu et al., 2014).

For a deeper understanding of the deformation mechanisms in GNG materials, the relationships between their microstructure and mechanical properties have been investigated by theoretical models and numerical simulation (Li et al., 2017; Lu et al., 2019; Moering et al., 2016; Wang et al., 2017; Zeng et al., 2016; Zhao et al., 2019; Zhao et al., 2020). On the one hand, some researchers studied the GNG IF steel by establishing constitutive models based on the conventional strain gradient of plasticity (Huang et al., 2004). These constitutive models involve the effects of various factors such as grain size, geometrically necessary dislocations (GNDs), and back stress (Li et al., 2017; Zhao et al., 2019; Zhao et al., 2020). On the other hand, the dislocation mechanism-based size-dependent crystal plasticity models have been employed to predict the tensile mechanical behavior of GNG material (Li and Yang, 2017; Lu et al., 2019; Zeng et al., 2016). The high strain hardening capability of GNG materials was attributed to the generation of abundant GNDs built up to accommodate the deformation incompatibility.

The studies mentioned above have discussed the deformation mechanism of GNG materials and predicted their yield strength, strain-hardening, and ductility. However, the analytical relations between structural gradient, strain gradient, and GND distribution for GNG materials are still unknown (Li et al., 2020). This issue may hinder the more profound understanding of the deformation mechanism in GNG materials. Besides, most previous studies focused on only one type of gradient structure. The understanding of the effect of different types of microstructures is limited. Recently, Lin et al. found the optimum grain size distribution of new GNG architectures by adopting electrodeposition to control the grain size and grain size gradient profile of nickel (Lin et al.,

E-mail address: yuli@imech.ac.cn.

https://doi.org/10.1016/j.ijsolstr.2022.111686
Received 17 September 2021; Received in revised form 28 March 2022; Accepted 29 April 2022
Available online 4 May 2022

2018). This study suggests that adjusting the GNG material microstructure is an effective way to toughen and strengthen materials. However, the study of the above GNG architectures is minimal due to the lack of an analytical relation between the structural gradient and mechanical properties. Therefore, it is necessary to develop a new theoretical model that contains the structure information, such as grain size distribution and grain size gradient. It is essential for designing GNG materials and optimizing their mechanical properties.

This paper is organized as follows. In Section 2, the postulates and basic formulas are described. The method for calculating the overall mechanical response of GNG materials is also introduced in this section. The corresponding predicted results and discussion of GNG IF-steel and Ni are given in Section 3.

2. The model description and formulations

Fig. 1(a) shows a schematic of the GNG plate sample. We assume that the grain size variation occurs only in the x-axis, that is $D = D(x)$. The generalized average grain size is related to the volume of grain V, that is $D = \sqrt[3]{V}$, obtained from experiments (Fang et al., 2011; Lin et al., 2018; Wu et al., 2014). In previous studies, GNG architecture has been usually treated as a multilayer composite, each layer of which is an equivalent homogenous microstructure (Li and Soh, 2012; Li et al., 2017; Zhao et al., 2019; Zhao et al., 2020). In this case, the strain gradient is obtained by the strain state of the adjacent homogenous layer. This paper still treats GNG architecture as a multilayer composite, but the grain size in each layer isn't homogenous. The average grain size and grain size gradient of the mesoscale representative volume element (RVE) of each layer can be expressed as $D(x_n)$ and $dD(x_n)/dx$, respectively. The relative multiscale framework schematic is shown in Fig. 1(b). Due to the gradient distribution of grain size, inherent heterogeneous deformation of RVE develops during deformation. Many GNDs are built up to accommodate the deformation incompatibility, leading to sustained strain hardening and enhanced ductility. We study the strain gradient in the RVE to reflect the effect induced by the structure gradient. In the following, we will first introduce the C-W strain gradient theory of plasticity (Chen and Wang, 2000) and the mechanical property of grain with different sizes. The relationship between the microstructure parameters ($D(x)$ and $dD(x)/dx$) and the strain gradient will be discussed subsequently.

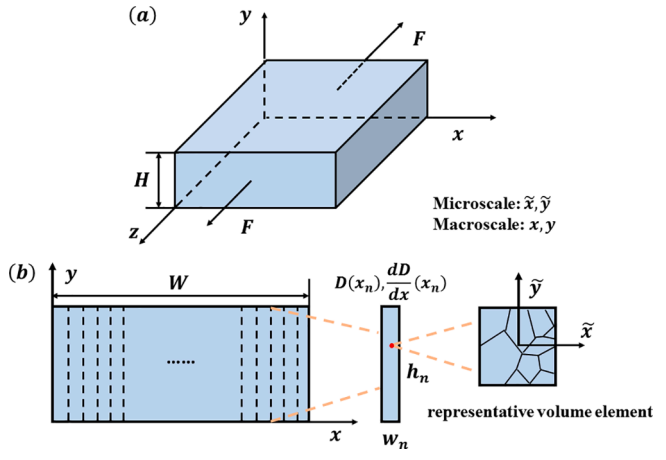

Fig. 1. (a) The schematic of the plate sample and the corresponding coordinate system. The sample is subjected to a tensile load parallel to the z-axis. (b) The plate sample is treated as a multilayer composite. The average grain size of each independent layer is $D(x)$, and the grain size gradient is $dD(x)/dx$. Due to the inhomogeneous microstructure, the strain gradient develops in the representative volume element during deformation. (x, y) and $(\tilde{x}, \tilde{y})$ are the coordinate of macroscale fields and mesoscale fields, respectively.

2.1. A theory framework of strain gradient plasticity

In the past few decades, many strain gradient theories have been put forward to explain the size effect of non-uniform deformation. The strain gradient of GNG samples under uniaxial tension is similar to the strain-gradient plasticity induced by applying a non-uniform deformation (such as bending, torsion). The micromechanisms of these two phenomena are related to the GND caused by non-uniform deformation. In recent years, many works (Li et al., 2017; Zhao et al., 2020) have been reported on the mechanical behavior of GNG materials based on the conventional strain gradient theory of plasticity (Huang et al., 2004). However, C-W theory (Chen and Wang, 2000) with concise form can better study the analytical relationship between structural gradient and strain gradient and mechanical properties.

The C-W theory involved strain gradient as an internal variable to describe the hardening behavior of materials under non-uniform deformation, which can be expressed as,

$$\dot{\sigma}_e = A^{'}(\varepsilon_e)\left(1 + \frac{l^2\eta^2}{\varepsilon_e^2}\right)^{\alpha}\dot{\varepsilon}_e = B(\varepsilon_e, l\eta)\dot{\varepsilon}_e. \tag{1}$$

Here, α in Eq. is a parameter ranging from 0 to 1. In this paper, $\alpha = 0.5$ is taken. $B = B(\varepsilon_e, l\eta)$ is the hardening function, including the effect of strain gradient. The l is an intrinsic material length in strain gradient plasticity. $\sigma_e = \sqrt{3\sigma_{ij}^{'}\sigma_{ij}^{'}/2}$ denotes the usual Von Mises effective stress, $\varepsilon_e = \sqrt{2\varepsilon_{ij}^{'}\varepsilon_{ij}^{'}/3}$ is the effective strain. $\sigma_{ij}^{'}$ and $\varepsilon_{ij}^{'}$ are deviatoric stress and strain, respectively. ε_{kk}, σ_{kk} are the mean strain and the hydrostatic stress. The η is the effective strain gradient,

$$\eta = \sqrt{\frac{2}{3}\chi_{ij}\chi_{ij} + c\eta_{ijk}^{(1)}\eta_{ijk}^{(1)}}, \tag{2}$$

where c is a dimensionless material parameter, $\chi_{ij} = e_{ikl}\varepsilon_{j,lk}$ is the curvature tensor, and $\eta_{ijk}^{(1)}\eta_{ijk}^{(1)}$ is the first quadratic invariant of the gradient $\varepsilon_{ij,k}$ (Fleck and Hutchinson, 1997, 2001). $A^{'}(\varepsilon_e)$ in Eq. is the tangent hardening modulus in the incremental version of conventional J_2 deformation theory. For power hardening materials, $A^{'}(\varepsilon_e)$ can be taken as.

$$A^{'}(\varepsilon_e) = N\Sigma_0\varepsilon_e^{N-1}, \tag{3}$$

with a reference stress $\Sigma_0 = \sigma_{eY}/\varepsilon_{eY}$. The σ_{eY} and ε_{eY} are the effective stress and the corresponding effective strain while material initial yields, respectively. N is a strain hardening exponent that is usually between 0 and 0.5.

2.2. The relationship between strain gradient and structure gradient

The previous researches show that grain size affects the mechanical properties of grain, such as yield strength and hardening ability (Carvalho Resende et al., 2013). The pioneering works of Hall and Petch enable the description of the yield stress of grain with different sizes (Hall, 1951; Petch, 1953),

$$\sigma_{eY} = \sigma_0 + \frac{k_Y}{\sqrt{D}}. \tag{4}$$

The σ_0 is the lattice friction stress, k_Y is the Hall-Petch slope, and D denotes the average grain size. Furthermore, to evaluate strain hardening exponent N for intermediate grain sizes, N is also assumed inversely proportional to the square root of the size of the local grain D (Zeng et al., 2016),

$$N = N_0 + \frac{k_N}{\sqrt{D}}, \tag{5}$$

where N_0 and k_N are fitting constants, which can be computed by ex-

periments (more discussion about this function are shown in Supplementary information). As shown in Fig. 1, the RVE with a gradient structure will produce a strain gradient while deformed due to the introduced size-dependent properties of grains. The value of the strain gradient rate in the RVE can be obtained by the following formula (the specific derivation can be seen in Appendix A),

$$\frac{d\dot{\varepsilon}_{ij}}{dx} = \frac{3}{2}\frac{\sigma'_{ij}}{\sigma_e}\frac{\dot{\sigma}_e}{B}C(\varepsilon_e)\left[\Omega(\varepsilon_e)\frac{dD}{dx} + \Pi(\varepsilon_e)\frac{d\varepsilon_e}{dx}\right], \tag{6}$$

where

$$\Omega(\varepsilon_e) = \frac{(1-N)}{\sigma_{eY}}\frac{d\sigma_{eY}}{dD} + \left[\ln\left(\frac{\sigma_{eY}}{3\mu\varepsilon_e}\right) - \frac{1}{N}\right]\frac{dN}{dD}, \tag{7}$$

$$\Pi(\varepsilon_e) = \frac{1+2\alpha-N}{\varepsilon_e} - 2\alpha\frac{\varepsilon_e}{\varepsilon_e^2 + l^2\eta^2}. \tag{8}$$

The dot denotes differentiation to time t and dx is space differential. The $C(\varepsilon_e) = \varepsilon_e/\varepsilon_{eY}$ reflects the constraint of the surrounding elements on RVE while the increase of strain gradient. Eq. describes the individual contribution of different mechanisms on the strain gradient. The $\Omega(\varepsilon_e)$ describes the effect of grain size gradient dD/dx on strain gradient. Specifically, the first term in $\Omega(\varepsilon_e)$ denotes the strain gradient caused by the difference in the yield strength of grains of different sizes, as shown in Fig. 2(a). The second term represents the strain gradient resulting from the difference in hardening ability, as shown in Fig. 2(b). The $\Pi(\varepsilon_e)$ describes the effect of the accumulation of strain gradient on the subsequent increment of strain gradient. Eq. provides the relationship between the strain gradient increment and average grain size, grain size gradient, and effective stress increment.

2.3. Calculation of overall mechanical response

The present study mainly focuses on the GNG plate sample subjected to uniaxial uniform strain ε_z^a (Lin et al., 2018; Wu et al., 2014). The loading in the calculation is strain-controlled in z-direction. The GNG structure is treated as a multilayer composite, and the strain component in z-direction of each layer is the same but different in other component, especially in the x-direction. We choose the volume average of all independent layers to approximately describe the overall stress–strain response of the GNG sample, similar to the rule of mixture (ROM) method (Li and Soh, 2012),

$$\sigma_z^G = \frac{\sum_{n=1}^{n^*}\sigma_{z(n)}h_n w_n}{HW}, \tag{9}$$

where σ_z^G denotes the overall stress–strain response and corresponds to the measured stress. $\sigma_{z(n)}$, h_n, w_n are the z-component stress, thickness, and width of layer n, respectively. H and W are the thickness and the width of the entire gradient sample, as shown in Fig. 1. The detail of the calculation of σ_z^G and σ_{zn} are shown in Appendix B. Finally, based on the calculated mechanical quantity, the Considere criterion is implemented to obtain the necking strain of samples, i.e., $d\sigma_z^G/d\varepsilon_z^a \le \sigma_z^G$.

3. Results and discussion

3.1. The mechanical response of gradient IF steels

In the above introduced constitutive model, the mechanical properties of each independent layer are closely related to its internal average grain size and grain size gradient. To a certain degree, the overall mechanical responses of GNG materials depend on their average grain size distribution function $D(x)$. Wu et al. fabricated a GNG IF-steel by SMAT and tested its tensile mechanical property (Wu et al., 2014). Quasi-static uniaxial tensile tests were carried out at a strain rate of $5 \times 10^{-4} \bullet s^{-1}$. For this gradient IF steels, the average grain size increases from 96 nm to 35 μm along the depth direction x, and the average grain size distribution function $D(x)$ can be approximately expressed as,

$$\log_{10}D(x) = \begin{cases} -1.03 + 2.9683\times10^{-5}x^{2.4} & x < 89 \\ 1.544 - 1.2576\times10^{-6}(x-120)^4 & 89 \leqslant x \leqslant 120 \\ \log_{10}120 & x > 120 \end{cases}. \tag{10}$$

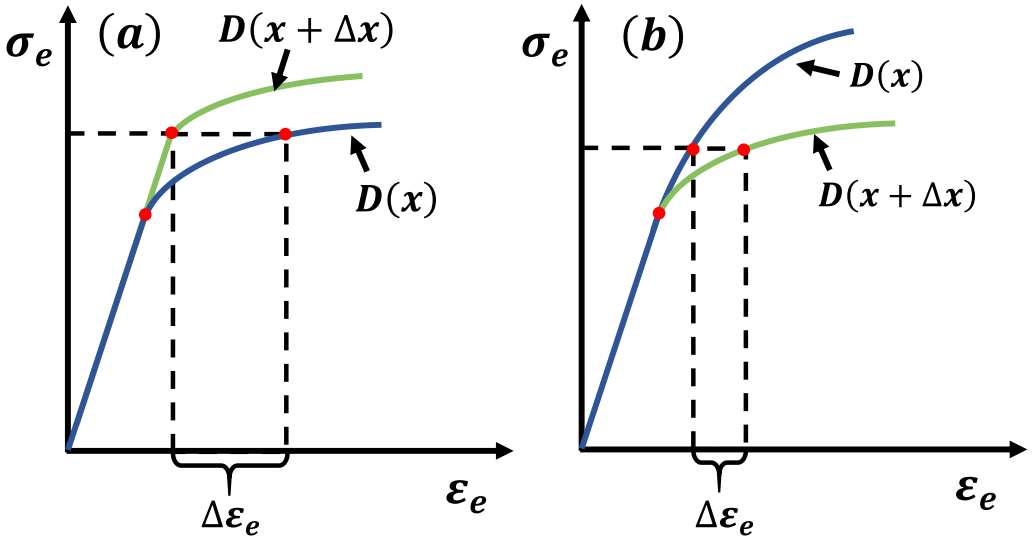

Fig. 2. Schematic diagram of the influence of grain size gradient in gradient structure element. (a) The influence of yield strength of grains of different sizes. (b) The influence of the difference in hardening ability.

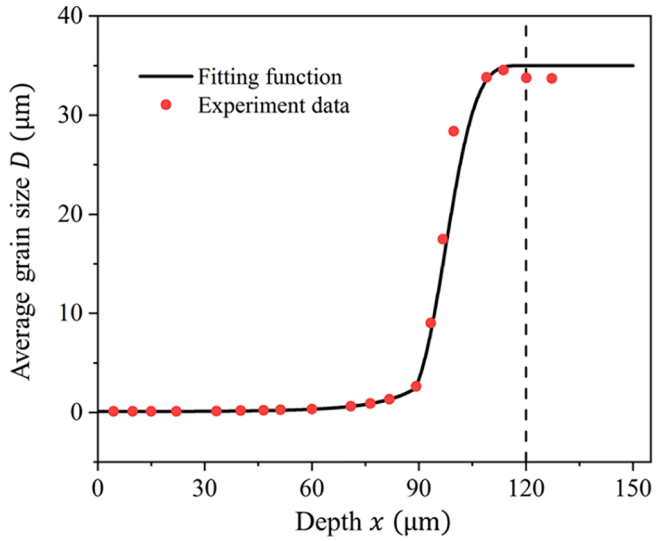

Fig. 3. The experimentally measured data and the fitting average grain size distribution continuous function.

Fig. 3 shows the fitting curve. It should be noted that the experimentally investigated IF-steel sheet has a dimension of 1000 μm × 2500 μm × 8000 μm ($x \times y \times z$). We selected half of the total sample to analyze to simplify the simulation, which means the variety range of × is 0 ∼ 500 μm.

Besides the grain size distribution function, it is necessary to obtain other constitutive parameters, such as elastic modulus E, Poisson's ratio ν, and the parameters σ_0 and k_Y in the Hall-Petch formula. The shear modulus and Poisson's ratio can be obtained from the literature (Li et al., 2017; Wu et al., 2014). The parameters in Hall-Petch formula Eq. and strain hardening exponent formula Eq. can be obtained by the stress–-strain curves of homogeneously-grained IF steel with the grain size of 96 nm and 650 nm (Li et al., 2017; Wu et al., 2014). The predicted true stress-true strain curves and corresponding experimental data for two samples with the grain size of 96 nm and 650 nm are shown in Fig. 4(a). It can be found that the predicted curves are in good agreement with the experimental data. The parameter values used in the calculation are listed in Table 1. The predicted overall mechanical response of gradient

Table 1
Material parameters for gradient IF steel samples.

Elastic modulus E (GPa)	Possion's ratio υ	Lattic frictional stress σ_0(MPa)	Hall-Petch slope k_Y(MPa/μm^2)
197	0.28	0.862	160.55
N_0	k_N	material length l(μm)	
0.3347	−0.1167	5	

IF steel is shown in Fig. 4(b), and the simulated results of other studies are also included for comparison. It turns out that the modeling prediction is in good agreement with the experiment stress–strain curve. Specifically, the predicted true uniform strain is 24%, similar to experiment one of 22%. The predicted ultimate tensile strength (true stress) of the GNG IF-steel is 363 MPa, which is 10 MPa higher than the experimental one. Finally, the results in this paper are also well comparable to those simulated results given in other published work. The above discussions indicate that the model in the present work can well describe the overall mechanical response of GNG IF-steel under uniaxial tension.

3.2. The optimal grain distribution profile of gradient grained nickel

The suitability of the present model has been validated by predicting the mechanical response of the GNG IF-steel in Section 3.1. This model can predict the overall mechanical response of GNG materials through the grain size and size gradient distribution. In this part, we applied this model to investigate the deformation behaviors of GNG materials with different microstructures. Recently, Lin et al. (Lin et al., 2018) found the optimum grain size distribution of new GNG architectures by adopting electrodeposition to control the grain size and grain size gradient profile of nickel. The grain size distribution of the prepared samples can be approximately regarded as changing along a single direction. They employed a power law equation to characterize the degree of the gradient in GNG Ni with different grain size profiles, as shown in Fig. 5. The average grain size D is related to normalized position $\bar{x}$,

$$D = D_{\max} - (D_{\max} - D_{\min})(1 - \bar{x})^n, \tag{11}$$

where n is the power index for the grain size distribution. The values of n of samples I to VI are 0.01, 0.016, 0.4, 0.75, 3, and 5, respectively. $\bar{x} = x/L$ is the normalized position, and L is the length of samples in the x-direction. $D_{max} = 4\mu m$ and $D_{min} = 29nm$ are the maximum and mini-

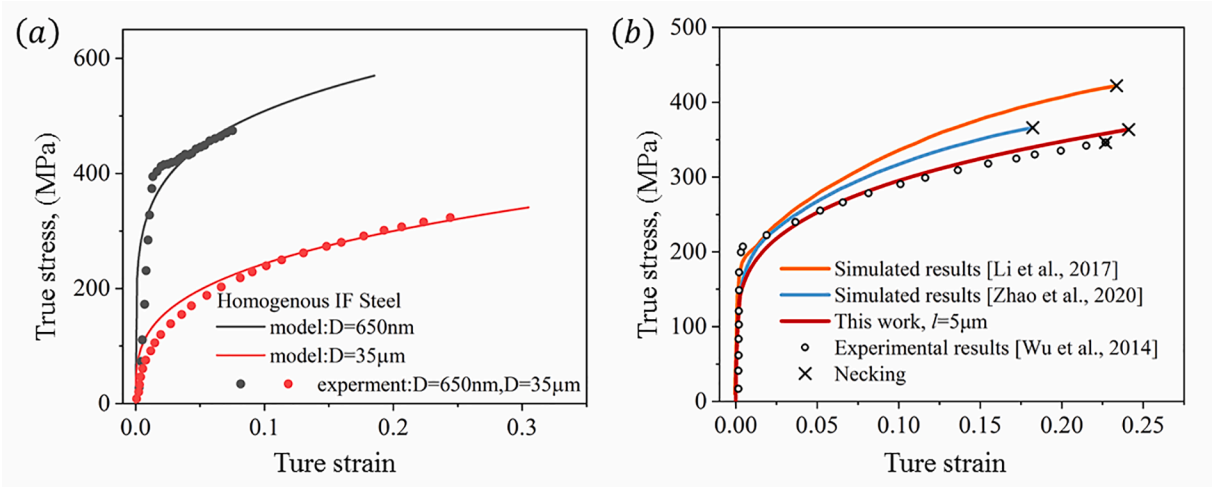

Fig. 4. (a) The predicted stress–strain curves of homogenous IF steel. The experiment data for $D = 650$ nm and $D = 35$ μm samples are included for comparison. (b) The predicted true stress–strain curves of gradient IF steel. The experiment and other simulated results are included for comparison. The cross symbols represent the necking in theoretical prediction and experiment.

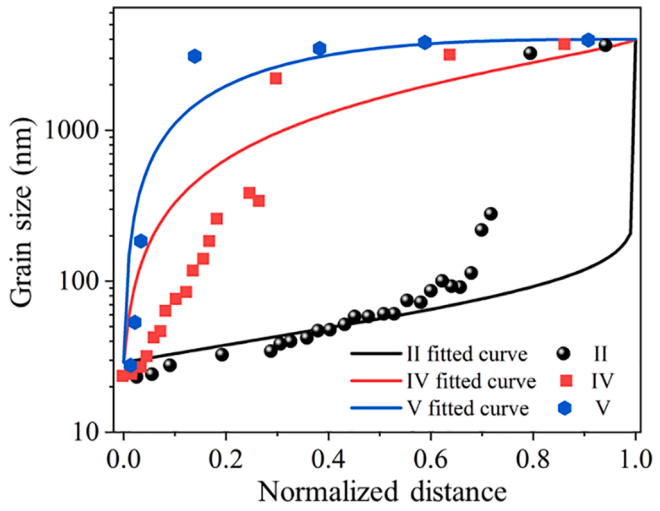

Fig. 5. Average grain size as a function of the normalized distance in sample II, IV and V, respectively (Lin et al., 2018).

Table 2
Material parameters for gradient grained nickel.

Elastic modulus E (GPa)	Possion's ratio υ	Lattic frictional stress σ_0(MPa)	Hall-Petch slope k_Y(MPa/μm^2)
207	0.291	405.3	169.4
N_0	k_N	material length l(μm)	
0.077	−0.008	10	

mum grain sizes, respectively. Quasi-static uniaxial tensile tests were carried out at a strain rate of $3 \times 10^{-4} s^{-1}$ at room temperature. The schematic diagram of the prepared samples and the loading direction can also be expressed in Fig. 1(a). The experiments show that both the yield stress and necking strain of sample V ($n = 3$) is enhanced as compared with their homogeneous counterparts.

Through the grain size distribution function provided in the experiment, the overall mechanical response of GNG Ni can be predicted. Table 2 shows the related parameters given by homogenous samples and one type of gradient sample. The stress–strain curve of sample V is chosen as a calibration curve to get material length l. For comparison, the calculated results of both homogenous and gradient structure samples are shown in Fig. 6. It displays tension stress–strain curves of the GNG Ni samples with different power indexes n before necking. As expected, the degree of the gradient has a strong effect on both strength and ductility. The results in Fig. 6(a) show the same strength-ductility trade-off as traditional materials when strain gradient effects are ignored. Besides, the strength of all samples except samples I and II is greatly underestimated. As shown in Fig. 6(b), the predicted results are more consistent with the experiment by considering the strain gradient effect. Compared with the former, the predicted strength of samples I and II increased slightly, while the prediction of other samples changed significantly.

Furthermore, we need to explain the deviation during elastic deformation and the initial plastic deformation stage in Fig. 6(b). Firstly, the previous studies (Mei et al., 2010) show that grain size also affects the elastic modulus of crystal materials, but this effect is not included in the existing theoretical model. The effect of elastic modulus is also reflected in this experiment. The stress–strain curves of each sample have separated before yield. Secondly, the average grain size function Eq. is a function based on the experiment data. It is not easy to completely accurate describe the real relationship between grain size and position. It is also worth mentioning that the above deviation does not qualitatively affect the trend of ultimate tensile strength and necking strain with different power indexes n (Supplementary information).

The variation curves of necking strain versus n and ultimate tensile strength versus necking strain are shown in Fig. 7(a) and (b), respectively. It includes the experiment data of samples I to VI and the corresponding theoretical prediction results. The experiment indicates that the true strain at which necking occurs reaches a peak value at $n = 3$ (sample V). Both necking strain and strength, in this case, are more prominent than that of the CG Ni sample. The model in this paper can well predict this phenomenon. It can be found that the predicted necking strain of sample VI is larger than the experimental data. The major reason is that the grain size changes dramatically in some regions, resulting in a large strain gradient between this region and the surrounding material. The larger strain gradient strengthens the material, restrains the deformation, and prevents the strain gradient from increasing. The simplified assumption of multilayered composite underestimates the interaction between layers (Li et al., 2017), resulting in the larger necking strain. However, considering the complicated gradient microstructure and other sample results, the predicted curves are reasonable to agree with the experiment data.

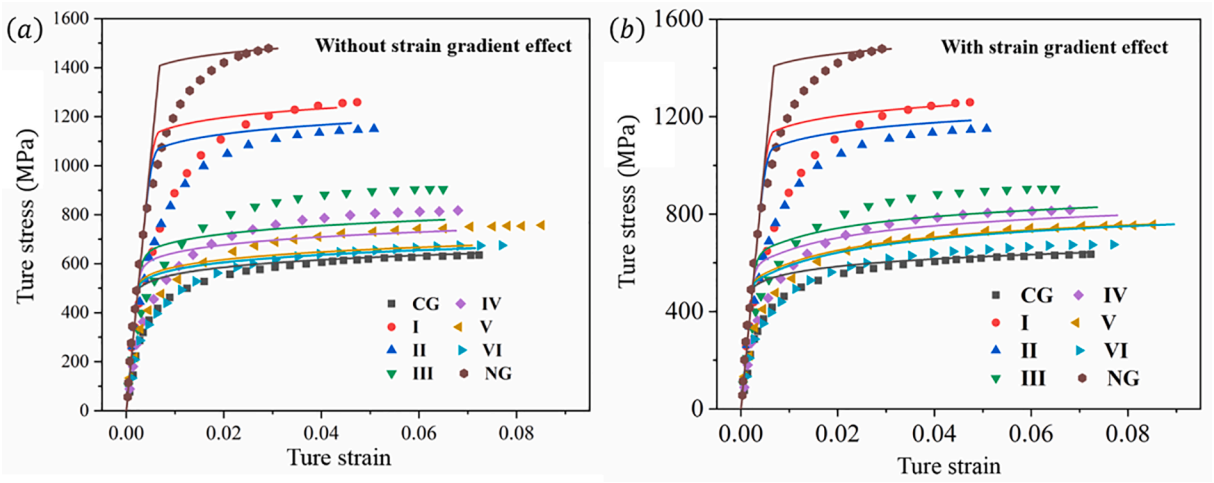

Fig. 6. (a) and (b) represent the tension stress–strain curves with and without considering the strain gradient effect, respectively. The points with different shapes represent the experiment data of samples with different values of n. The lines of the same color corresponding to these points are theoretical calculation results. Both (a) and (b) only show the experimental and calculation results during uniform deformation.

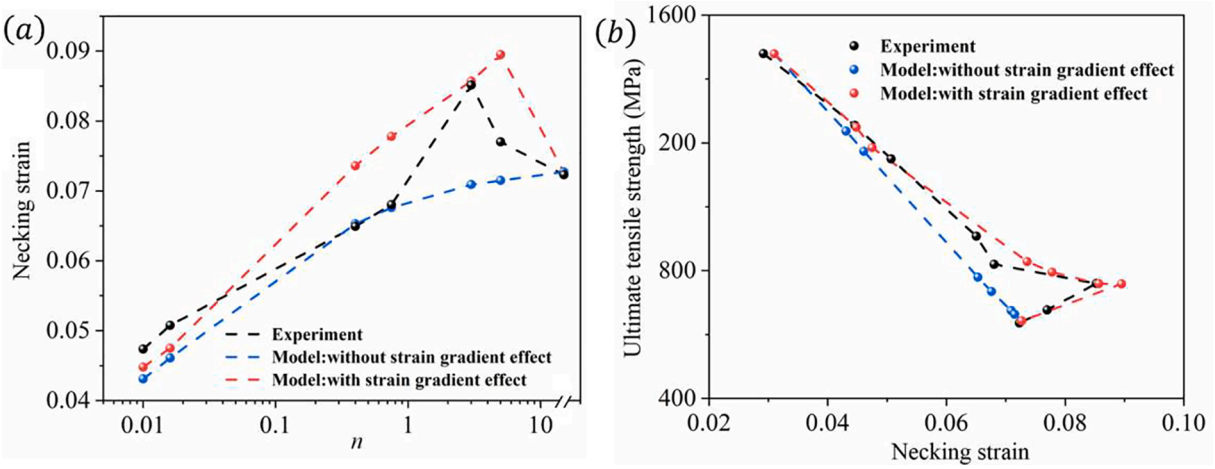

Fig. 7. (a) Necking strain as a function of *n*. (b) Ultimate tensile strength versus necking strain for electrodeposited CG, NG, and various GNG Ni. Both theoretical prediction results and experimental data are included in the figure. The dash lines are only the connecting line of each sample point.

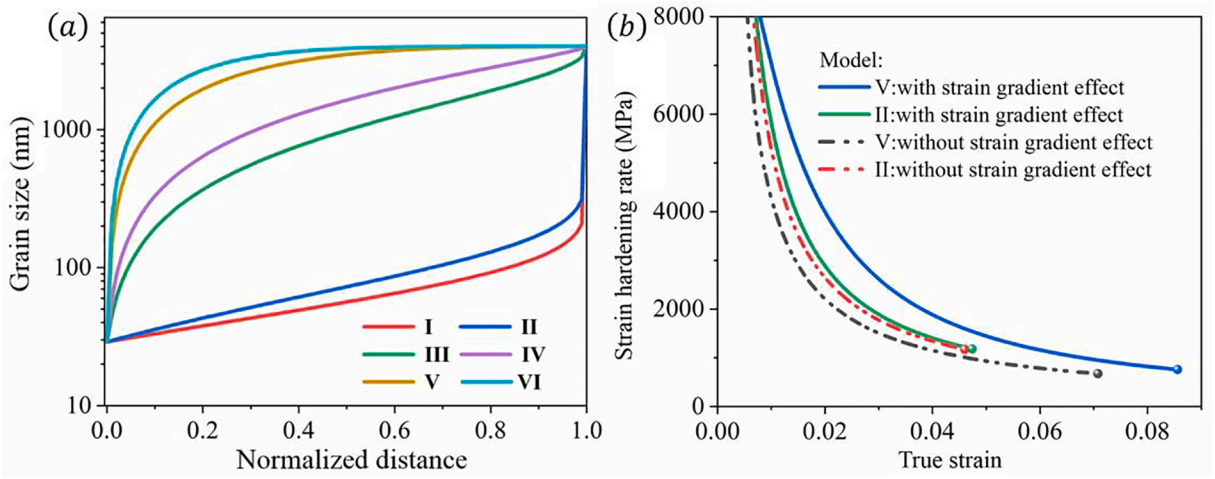

Fig. 8. (a) Average grain size function of sample I to VI. (b) The predicted strain hardening rate for samples II and V. The results with and without strain gradient effect are included in (b) for comparison.

3.3. Discussion

The above results have shown that the strain gradient induced by heterogeneous structure plays a substantial effect on the mechanical property of GNG material. The strain gradient is directly related to the grain size and grain size distribution profile. The average grain size function Eq. is shown in Fig. 8(a). The diagram shows that the volume fraction of CG in the sample increases with the increase of *n*. The curves of samples II and V have similar profiles, including gentle and severe variation parts. However, it can be found from Fig. 8(b) that the strengthening effect of the gradient structure in sample II is much lower than that in sample V.

On the one hand, the solid green line and red dash line in Fig. 8(b) describe the variation of strain hardening rate with and without considering the strain gradient effect, respectively. These two lines almost coincide. On the other hand, due to the effect of the gradient structure, the strain hardening rate of sample V is greatly improved, and a larger uniform strain is obtained. It can be found from Eq. that the strain gradient in GNG is not only related to the grain size gradient but also related to the accumulated strain gradient. For the results in Fig. 8 (a), sample V contains more coarse-grained soft phases than sample II. The decrease of strength of sample V results in good deformation ability, which is more conducive to the development of strain gradient. For GNG

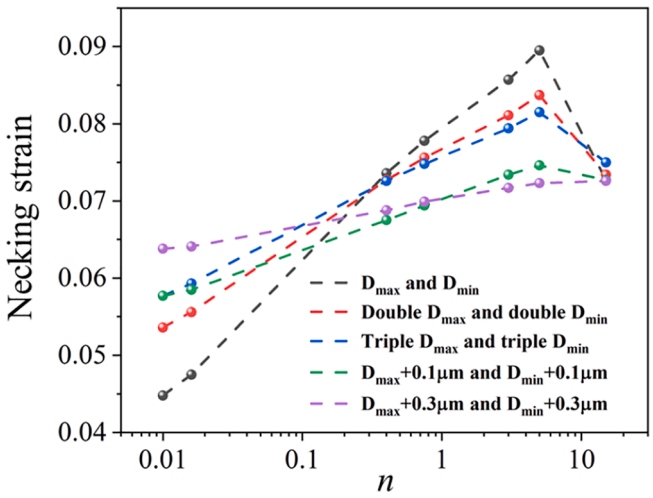

Fig. 9. Necking strain as a function of *n*. The black dash line corresponds to the original data. The red and blue dash lines magnify the minimum and maximum grain size by 2 and times, respectively. The green and purple dash lines increase the minimum and maximum grain sizes by 0.1 μm and 0.3 μm.

materials, the nano-grains play an essential role in improving strength, while the coarse grain is the primary carrier of deformation. It is an effective way to strengthen and toughen materials to reasonably adjust the composition and distribution of nano-grains and coarse grains, such as lamellar structure (He et al., 2017; Huang et al., 2016; Wu and Zhu, 2017), harmonic structure (Ma and Zhu, 2017; Vajpai et al., 2016).

Fig. 9 shows the variation of necking strain with n when the grain size varies from nanometer scale to the micron/submicron scale. The black dash line corresponds to the original data. The Red and blue dash lines magnify the minimum and maximum grain size by two and three times, respectively. The green and purple dash lines increase the minimum and maximum grain sizes by 0.1 μm and 0.3 μm. The results show that with the increase of grain size, the influence of structural gradient is weakening. When the grain size increases exponentially, the size gap between the maximum and minimum grains becomes larger. When the grain size increases at the same time, the difference between them remains unchanged.

The present model provides a reference for the microstructure design of GNG material and quickly predicts its mechanical properties. The average grain size is essential in the whole work and the key to designing material microstructure. The average grain size function needs to be continuously derivable and can accurately reflect the microstructure of the sample. If there is a sharp variation of grain size similar to an interface in materials, it may lead to the singularity of the grain size function, and this model may estimate the stress–strain curve inaccurately. In addition, many works have reported that inverse Hall-Petch relation exists when the grain is reduced to a critical size (about tens of nanometers) (Chokshi et al., 1989; Schiøtz and Jacobsen, 2003). Therefore, this model is limited to study the case that the grain size is smaller than the critical size.

4. Conclusions

This paper treats the GNG materials as a multilayer composite with the intra-layer grain size gradient. A constitutive model is developed to predict the overall mechanical response of GNG materials based on grain size distribution profile. The main results are summarized as follows:

(1) The analytical relation between the strain gradient, average grain size, and grain size gradient in GNG materials is explored. The difference in yield strength and hardening ability of grains with different sizes, as well as the accumulated strain gradient, will affect the increment of strain gradient.
(2) The predicted true stress–strain curves of gradient IF steel samples agree with the experimental results and are comparable with the simulated results of other works. The strength-ductility performance of GNG samples is remarkably enhanced as compared with their homogeneous counterparts.
(3) According to the grain size distribution function of several GNG Ni, the corresponding true stress–strain curves, uniform strain, and ultimate tensile strength are obtained. The model successfully predicts the synchronous increase of strength and necking strain of sample V, consistent with the experiment.
(4) The strength-ductility performance of GNG samples can be further improved by adjusting their microstructure. The model in the present paper provides references for the microstructure design.

Declaration of Competing Interest

The authors declare that they have no known competing financial interests or personal relationships that could have appeared to influence the work reported in this paper.

Acknowledgments

The author is grateful to Prof. Tzu-Chiang Wang and Dr. Feng Liu for their fruitful discussion and insightful comments. This work was financially supported by the National Natural Science Foundation of China (Grant Nos. 11790292) and the Strategic Priority Research Program of the Chinese Academy of Sciences (Grant No. XDB22040503).

Appendix A

As shown in Fig. 1(b), the RVE with gradient structure is accompanied by non-uniform deformation even under a uniform external field. The micro strain in RVE can be expressed as $\widetilde{\varepsilon}_{ij}(\widetilde{x})$ (the grain size gradient distribution along the x-axis only) that can be divided into the deviatoric strain and mean strain,

$$\widetilde{\varepsilon}_{ij} = \widetilde{\varepsilon}'_{ij} + \delta_{ij}\frac{\widetilde{\varepsilon}_{kk}}{3} = \frac{3}{2}\frac{\widetilde{\varepsilon}_e}{\widetilde{\sigma}_e}\widetilde{\sigma}'_{ij} + \frac{1}{9K}\delta_{ij}\widetilde{\sigma}_{kk} \tag{A.1}$$

where K is the bulk modulus, δ_{ij} is Kronecker's delta. We assume that the internal stress of RVE is distributed uniformly, then $\widetilde{\sigma}_e$, $\widetilde{\sigma}_{kk}$, $\widetilde{\sigma}_{ij}$ are unchanged with the position in the element. However, the total strain in the element will change with $\widetilde{x}$ because of the gradient structure. As shown in Fig. A1, we regard the RVE with gradient as a combination of two uniform parts, similar to the model of multilayer composite. The mechanical responses of these two parts are calculated independently by the isotropic theory. In this case, the strain gradient of the two parts in RVE can be expressed as,

$$\frac{d\widetilde{\varepsilon}_{ij}}{d\widetilde{x}} = \frac{3}{2}\frac{\widetilde{\sigma}'_{ij}}{\widetilde{\sigma}_e}\frac{d\widetilde{\varepsilon}_e}{d\widetilde{x}}. \tag{A.2}$$

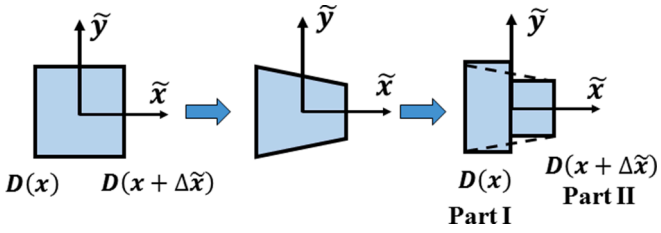

Fig. A1. Schematic diagram of model. (x,y) and $(\widetilde{x},\widetilde{y})$ are the coordinate of macro fields and micro fields, respectively.

The incremental form about time of Eq. is.

$$\frac{d\dot{\widetilde{\varepsilon}}_{ij}}{d\widetilde{x}}=\frac{3}{2}\left(\frac{\dot{\widetilde{\sigma}}'_{ij}}{\widetilde{\sigma}_e}-\frac{\widetilde{\sigma}'_{ij}\dot{\widetilde{\sigma}}_e}{\widetilde{\sigma}_e^2}\right)\frac{d\widetilde{\varepsilon}_e}{d\widetilde{x}}+\frac{3}{2}\frac{\widetilde{\sigma}'_{ij}}{\widetilde{\sigma}_e}\frac{d\dot{\widetilde{\varepsilon}}_e}{d\widetilde{x}}, \tag{A.3}$$

where the dot denotes differentiation with respect to time t. For C-W strain gradient theory, the effective strain rate $\dot{\widetilde{\varepsilon}}_e$ can be obtained from hardening law Eq.,

$$\dot{\widetilde{\varepsilon}}_e = \frac{1}{A'\left(\widetilde{\varepsilon}_e\right)}\left(1+\frac{l^2\eta^2}{\widetilde{\varepsilon}_e^2}\right)^{-\alpha}\dot{\widetilde{\sigma}}_e = \frac{1}{B}\dot{\widetilde{\sigma}}_e. \tag{A.4}$$

Then, the expression of $d\dot{\widetilde{\varepsilon}}_e/d\widetilde{x}$ can be obtained,

$$\frac{d\dot{\widetilde{\varepsilon}}_e}{d\widetilde{x}}=-\frac{\dot{\widetilde{\sigma}}_e}{B^2}\frac{dB}{d\widetilde{x}}=\frac{\dot{\widetilde{\sigma}}_e}{B}\left[\Omega\left(\widetilde{\varepsilon}_e\right)\frac{dD}{d\widetilde{x}}+\Pi\left(\widetilde{\varepsilon}_e\right)\frac{d\widetilde{\varepsilon}_e}{d\widetilde{x}}\right], \tag{A.5}$$

where.

$$\Omega\left(\widetilde{\varepsilon}_e\right)=\frac{(1-N)}{\sigma_{eY}}\frac{d\sigma_{eY}}{dD}+\left[\ln\left(\frac{\sigma_{eY}}{3\mu\widetilde{\varepsilon}_e}\right)-\frac{1}{N}\right]\frac{dN}{dD}, \tag{A.6}$$

$$\Pi\left(\widetilde{\varepsilon}_e\right)=\frac{1+2\alpha-N}{\widetilde{\varepsilon}_e}-2\alpha\frac{\widetilde{\varepsilon}_e}{\widetilde{\varepsilon}_e^2+l^2\eta^2}. \tag{A.7}$$

D is the average grain size of RVE, and σ_{eY} and N are the corresponding yield strength and strain hardening exponent, respectively. η is the strain gradient in RVE. Finally, the stress state and strain state of microscale fields and mesoscale fields can be linked by the plastic work equivalence,

$$\dot{\varepsilon}_{ij}=\frac{1}{V}\int_V\dot{\widetilde{\varepsilon}}_{ij}dV, \qquad \sigma_{ij}=\frac{1}{V}\int_V\widetilde{\sigma}_{ij}dV. \tag{A.8}$$

By combining Eq. (A.5), (A.8), and (A.3) and ignoring the high order small quantity, the following equation is given,

$$\frac{d\dot{\varepsilon}_{ij}}{dx}=\frac{3}{2}\left(\frac{\dot{\sigma}'_{ij}}{\sigma_e}-\frac{\sigma'_{ij}\dot{\sigma}_e}{\sigma_e^2}\right)\frac{d\varepsilon_e}{dx}+\frac{3}{2}\frac{\sigma'_{ij}}{\sigma_e}\frac{\dot{\sigma}_e}{B}\left[\Omega(\varepsilon_e)\frac{dD}{dx}+\Pi(\varepsilon_e)\frac{d\varepsilon_e}{dx}\right]. \tag{A.9}$$

The layers in this work are assumed to be independent, thus each independent layer considers the applied load in the z-direction only. The interaction of different layers may quantitatively change the strain gradient of each layer, but it doesn't make the enhancement effect of the strain gradient disappear. Therefore, the assumption of an independent layer doesn't qualitatively influence the results. In this case, the first part in Eq. equals zero. Furthermore, the macroscopic stress of RVE is given by plastic work equivalence. However, there is still non-uniform deformation in RVE. The non-uniform deformation is limited by the surrounding elements. This statement can be understood by studying two adjacent RVE. The grain size gradient leads to non-uniform deformation in RVE. The places with larger deformation of adjacent elements may squeeze each other, while the places with small deformation will pull each other, so as to resist the intensification of strain gradient. At the micro-level, GNDs accumulate with the deformation, and the large number of GNDs will hinder the formation of new GNDs. Therefore, the increase of strain gradient is gradually limited with the deformation. We introduce the $C(\varepsilon_e)=\varepsilon_e/\varepsilon_{eY}$ to describe this effect. Then, the result can be rewritten as,

$$\frac{d\dot{\varepsilon}_{ij}}{dx}=\frac{3}{2}\frac{\sigma'_{ij}}{\sigma_e}\frac{\dot{\sigma}_e}{B}C(\varepsilon_e)\left[\Omega(\varepsilon_e)\frac{dD}{dx}+\Pi(\varepsilon_e)\frac{d\varepsilon_e}{dx}\right]. \tag{A.10}$$

Appendix B

The $\sigma_{z(n)}$ of each layer and σ_z^G can be obtained as follows. The most important is calculating the increment of each mechanical quantity through strain increment in the z-direction (strain-controlled) according to the current stress and strain state. The strain component of layer n can be expressed as,

$$\varepsilon_{ij(n)}=\varepsilon'_{ij(n)}+\delta_{ij}\frac{\varepsilon_{kk(n)}}{3}=\frac{3}{2}\frac{\varepsilon_{e(n)}}{\sigma_{e(n)}}\sigma'_{ij(n)}+\frac{1}{9K}\delta_{ij}\sigma_{kk(n)}. \tag{B.1}$$

The incremental form of the above formula is,

$$\dot{\varepsilon}_{ij(n)}=\frac{3}{2}\left(\frac{\sigma'_{ij(n)}}{\sigma_{e(n)}}\dot{\varepsilon}_{e(n)}+\frac{\varepsilon_{e(n)}}{\sigma_{e(n)}}\dot{\sigma}'_{ij(n)}-\frac{\varepsilon_{e(n)}\sigma'_{ij(n)}}{\sigma_{e(n)}^2}\dot{\sigma}_{e(n)}\right)+\frac{1}{9K}\delta_{ij}\dot{\sigma}_{kk(n)}. \tag{B.2}$$

The layers are assumed to be independent, thus each independent layer needs to consider the applied load in the z-direction only. Thus $\sigma_{e(n)}=\sigma_{z(n)}$ and the above equation in the z-direction can be rewritten as,

$$\dot{\varepsilon}_{ij(n)}=\frac{3}{2}\frac{\sigma'_{ij(n)}}{\sigma_{e(n)}}\dot{\varepsilon}_{e(n)}+\frac{1}{9K}\delta_{ij}\dot{\sigma}_{kk(n)}=\left(\frac{3}{2}\frac{\sigma'_{ij(n)}}{\sigma_{e(n)}}\frac{1}{B_n}+\frac{1}{9K}\delta_{ij}\right)\dot{\sigma}_{e(n)}. \tag{B.3}$$

The effective stress can be obtained by Eq.,

$$\dot{\sigma}_{e(n)} = \dot{\sigma}_{z(n)} = \dot{\varepsilon}_{z(n)} / \left(\frac{1}{B_n} + \frac{1}{9K} \delta_{ij} \right). \tag{B.4}$$

This equation shows the increment relation between effective stress and strain in the z-direction of the layer n. B_n can reflect the effect of structure gradient of the different layers. The variation of effective strain and strain gradient in B_n can be given based on the effective stress increment by Eq., and. The stress and strain state of each layer can be obtained in this way. Then, updating the deformation state of the layer based on the calculated increment and carrying out the next iteration, the complete stress–strain curve can be shown.

Appendix C. Supplementary data

Supplementary data to this article can be found online at https://doi.org/10.1016/j.ijsolstr.2022.111686.

References

Carvalho Resende, T., Bouvier, S., Abed-Meraim, F., Balan, T., Sablin, S.S., 2013. Dislocation-based model for the prediction of the behavior of b.c.c. materials – Grain size and strain path effects. Int. J. Plast. 47, 29–48.

Chen, S.H., Wang, T.C., 2000. A new hardening law for strain gradient plasticity. Acta Mater. 48, 3997–4005.

Cheng, Z., Zhou, H., Lu, Q., Gao, H., Lu, L., 2018. Extra strengthening and work hardening in gradient nanotwinned metals. Science 362.

Chokshi, A., Rosen, A., Karch, J., Gleiter, H., 1989. On the validity of the Hall-Petch relationship in nanocrystalline materials. Scr. Metall. 23, 1679–1683.

Fang, T.H., Li, W.L., Tao, N.R., Lu, K., 2011. Revealing extraordinary intrinsic tensile plasticity in gradient nano-grained copper. Science 331, 1587–1590.

Fleck, N.A., Hutchinson, J.W., 1997. Strain gradient plasticity. Adv. Appl. Mech. 33, 295–361.

Fleck, N.A., Hutchinson, J.W., 2001. A reformulation of strain gradient plasticity. J. Mech. Phys. Solids 49, 2245–2271.

Hall, E.O., 1951. The Deformation and Ageing of Mild Steel: III Discussion of Results. Proc. Phys. Soc. London, Sect. B 64, 747–753.

He, B.B., Hu, B., Yen, H.W., Cheng, G.J., Wang, Z.K., Luo, H.W., Huang, M.X., 2017. High dislocation density–induced large ductility in deformed and partitioned steels. Science 357, 1029.

Huang, M., Fan, G.H., Geng, L., Cao, G.J., Du, Y., Wu, H., Zhang, T.T., Kang, H.J., Wang, T.M., Du, G.H., Xie, H.L., 2016. Revealing extraordinary tensile plasticity in layered Ti-Al metal composite. Sci. Rep. 6, 38461.

Huang, Y., Qu, S., Hwang, K.C., Li, M., Gao, H., 2004. A conventional theory of mechanism-based strain gradient plasticity. Int. J. Plast. 20, 753–782.

Li, J., Soh, A.K., 2012. Modeling of the plastic deformation of nanostructured materials with grain size gradient. Int. J. Plast. 39, 88–102.

Li, J., Weng, G.J., Chen, S., Wu, X., 2017. On strain hardening mechanism in gradient nanostructures. Int. J. Plast. 88, 89–107.

Li, X., Lu, L., Li, J., Zhang, X., Gao, H., 2020. Mechanical properties and deformation mechanisms of gradient nanostructured metals and alloys. Nat. Rev. Mater. 5, 706–723.

Li, Z., Yang, F., 2017. Grain rotations during uniaxial deformation of gradient nano-grained metals using crystal plasticity finite element simulations. Extreme Mech. Lett. 16, 41–48.

Lin, Y., Pan, J., Zhou, H.F., Gao, H.J., Li, Y., 2018. Mechanical properties and optimal grain size distribution profile of gradient grained nickel. Acta Mater. 153, 279–289.

Long, J., Pan, Q., Tao, N., Dao, M., Suresh, S., Lu, L., 2019. Improved fatigue resistance of gradient nanograined Cu. Acta Mater. 166, 56–66.

Lu, K., 2014. Making strong nanomaterials ductile with gradients. Science 345, 1455–1456.

Lu, X., Zhang, X., Shi, M., Roters, F., Kang, G., Raabe, D., 2019. Dislocation mechanism based size-dependent crystal plasticity modeling and simulation of gradient nano-grained copper. Int. J. Plast. 113, 52–73.

Ma, E., Zhu, T., 2017. Towards strength–ductility synergy through the design of heterogeneous nanostructures in metals. Mater. Today 20, 323–331.

Mei, Q.S., Zhang, L., Tsuchiya, K., Gao, H., Ohmura, T., Tsuzaki, K., 2010. Grain size dependence of the elastic modulus in nanostructured NiTi. Scr. Mater. 63, 977–980.

Moering, J., Ma, X., Malkin, J., Yang, M., Zhu, Y., Mathaudhu, S., 2016. Synergetic strengthening far beyond rule of mixtures in gradient structured aluminum rod. Scr. Mater. 122, 106–109.

Petch, N., 1953. The cleavage strength of polycrystals. J. Iron Steel Inst. Lond. 173, 25.

Schiøtz, J., Jacobsen, K.W., 2003. A maximum in the strength of nanocrystalline copper. Science 301, 1357–1359.

Shao, C.W., Zhang, P., Zhu, Y.K., Zhang, Z.J., Pang, J.C., Zhang, Z.F., 2017. Improvement of low-cycle fatigue resistance in TWIP steel by regulating the grain size and distribution. Acta Mater. 134, 128–142.

Vajpai, S.K., Ota, M., Zhang, Z., Ameyama, K., 2016. Three-dimensionally gradient harmonic structure design: an integrated approach for high performance structural materials. Materials Research Letters 4, 191–197.

Wang, Y., Yang, G., Wang, W., Wang, X., Li, Q., Wei, Y., 2017. Optimal stress and deformation partition in gradient materials for better strength and tensile ductility: a numerical investigation. Sci. Rep. 7, 10954.

Wei, Y., Li, Y., Zhu, L., Liu, Y., Lei, X., Wang, G., Wu, Y., Mi, Z., Liu, J., Wang, H., Gao, H., 2014. Evading the strength–ductility trade-off dilemma in steel through gradient hierarchical nanotwins. Nat. Commun. 5, 3580.

Wu, H., Fan, G., 2020. An overview of tailoring strain delocalization for strength-ductility synergy. Prog. Mater Sci. 113, 100675.

Wu, X., Jiang, P., Chen, L., Yuan, F., Zhu, Y.T., 2014. Extraordinary strain hardening by gradient structure. Proc. Natl. Acad. Sci. 111, 7197.

Wu, X., Zhu, Y., 2017. Heterogeneous materials: a new class of materials with unprecedented mechanical properties. Mater. Res. Lett. 5, 527–532.

Wu, X., Zhu, Y., Lu, K., 2020. Ductility and strain hardening in gradient and lamellar structured materials. Scr. Mater. 186, 321–325.

Zeng, Z., Li, X., Xu, D., Lu, L., Gao, H., Zhu, T., 2016. Gradient plasticity in gradient nano-grained metals. Extreme Mech. Lett. 8, 213–219.

Zhao, J., Kan, Q., Zhou, L., Kang, G., Fan, H., Zhang, X., 2019. Deformation mechanisms based constitutive modelling and strength-ductility mapping of gradient nano-grained materials. Mater. Sci. Eng., A 742, 400–408.

Zhao, J., Lu, X., Yuan, F., Kan, Q., Qu, S., Kang, G., Zhang, X., 2020. Multiple mechanism based constitutive modeling of gradient nanograined material. Int. J. Plast. 125, 314–330.